Seasonal changes in leaf area of Amazon forests from leaf flushing and abscission

Arindam Samanta,[1,2] Yuri Knyazikhin,[1] Liang Xu,[1] Robert E. Dickinson,[3] Rong Fu,[3] Marcos H. Costa,[4] Sassan S. Saatchi,[5] Ramakrishna R. Nemani,[6] and Ranga B. Myneni[1]

Received 18 July 2011; revised 23 November 2011; accepted 1 December 2011; published 11 February 2012.

[1] A large increase in near-infrared (NIR) reflectance of Amazon forests during the light-rich dry season and a corresponding decrease during the light-poor wet season has been observed in satellite measurements. This increase has been variously interpreted as seasonal change in leaf area resulting from net leaf flushing in the dry season or net leaf abscission in the wet season, enhanced photosynthetic activity during the dry season from flushing new leaves and as change in leaf scattering and absorption properties between younger and older leaves covered with epiphylls. Reconciling these divergent views using theory and observations is the goal of this article. The observed changes in NIR reflectance of Amazon forests could be due to similar, but small, changes in NIR leaf albedo (reflectance plus transmittance) resulting from the exchange of older leaves for newer ones, but with the total leaf area unchanged. However, this argument ignores accumulating evidence from ground-based reports of higher leaf area in the dry season than the wet season, seasonal changes in litterfall and does not satisfactorily explain why NIR reflectance of these forests decreases in the wet season. More plausibly, the increase in NIR reflectance during the dry season and the decrease during the wet season would result from changes in both leaf area and leaf optical properties. Such change would be consistent with known phenological behavior of tropical forests, ground-based reports of seasonal changes in leaf area, litterfall, leaf optical properties and fluxes of evapotranspiration, and thus, would reconcile the various seemingly divergent views.

Citation: Samanta, A., Y. Knyazikhin, L. Xu, R. E. Dickinson, R. Fu, M. H. Costa, S. S. Saatchi, R. R. Nemani, and R. B. Myneni (2012), Seasonal changes in leaf area of Amazon forests from leaf flushing and abscission, *J. Geophys. Res.*, *117*, G01015, doi:10.1029/2011JG001818.

1. Introduction

[2] The spectral signatures of Amazon forests as measured by passive optical satellite sensors such as the Moderate Resolution Spectroradiometer (MODIS) are characterized by two distinguishing features, strong scattering in the near-infrared (NIR) from internal-leaf cellular structures, and equally strong absorption in the shorter red and blue wavelengths from chlorophyll and other pigments vital to the process of photosynthesis. The NIR reflectance, the fraction of incident solar radiation at NIR wavelengths reflected by a surface, of these forests is an order of magnitude greater than the reflectance at red and blue wavelengths (Figure 1 and Figure S1 in the auxiliary material), and in any given year, increases by about 23% during the dry season and similarly decreases during the following wet season (Figure 1) [also *Asner et al.*, 2004].[1] This large increase in NIR reflectance of Amazon forests during the light-rich dry season has been variously interpreted, but generally characterized as from a greening of the Amazon forests during the dry season [*Huete et al.*, 2006; *Xiao et al.*, 2006; *Brando et al.*, 2010; *Myneni et al.*, 2007]. The objective of this paper is to harmonize these divergent interpretations of dry season greening of Amazon forests.

[3] The MODIS Enhanced Vegetation Index (EVI) is defined by an algebraic manipulation of vegetation reflectances at NIR, red and blue wavelengths [*Huete et al.*, 2002]. It is principally sensitive to NIR reflectance, as one can readily deduce from its formulation (cf. Section 3.3, equation (4)). Not surprisingly, the EVI displays higher values in the late dry season compared to the wet season or early dry season [*Huete et al.*, 2006; *Xiao et al.*, 2006;

[1]Department of Geography and Environment, Boston University, Boston, Massachusetts, USA.
[2]Atmospheric and Environmental Research Inc., Lexington, Massachusetts, USA.
[3]Department of Geological Sciences, University of Texas at Austin, Austin, Texas, USA.
[4]Agricultural and Environmental Engineering, Federal University of Viçosa, Vicosa, Brazil.
[5]Jet Propulsion Laboratory, California Institute of Technology, Pasadena, California, USA.
[6]Biospheric Sciences Branch, NASA AMES Research Center, Moffett Field, California, USA.

0148-0227/12/2011JG001818

[1]Auxiliary materials are available in the HTML. doi:10.1029/2011JG001818.

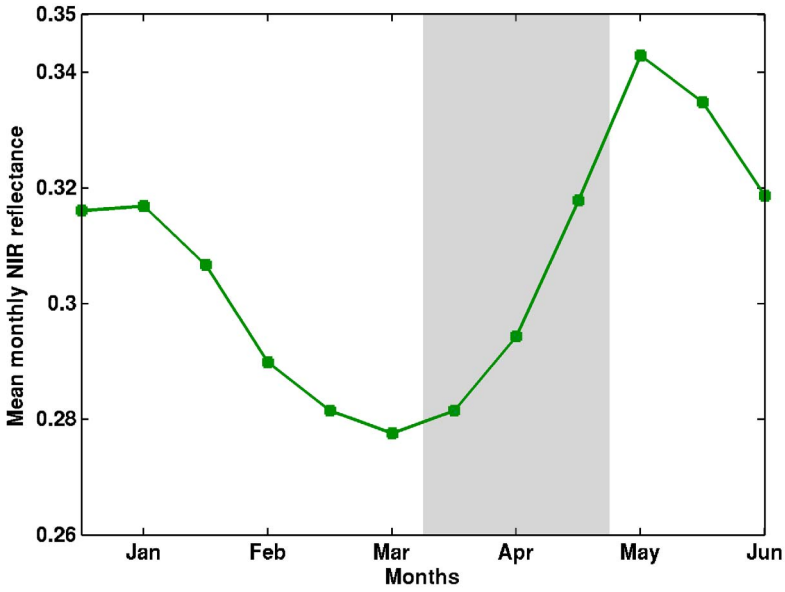

Figure 1. Monthly mean near-infrared (NIR) reflectance over forests, in the Amazon region 0°–20°S and 80°–40°W, with statistically significant green-up from June to October during 2000–2009 (Figure 6a).

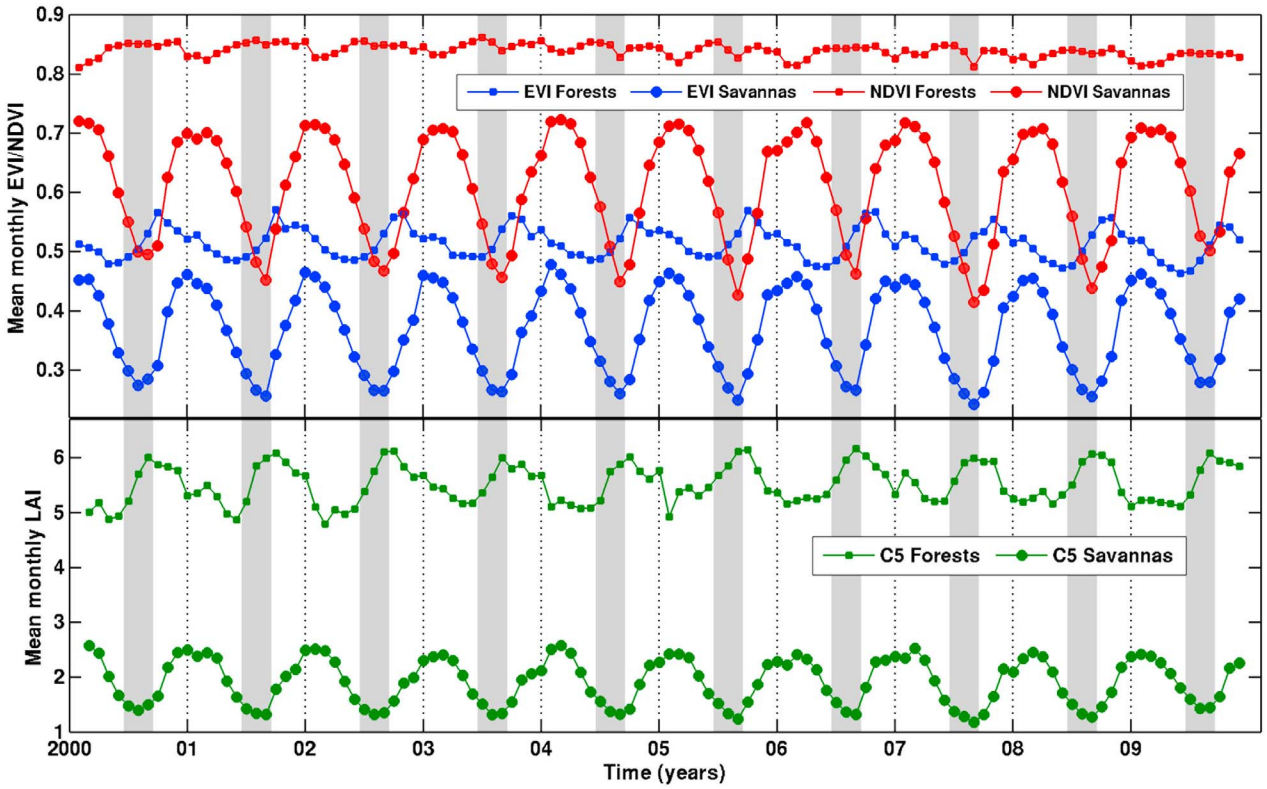

Figure 2. Monthly time series of EVI, NDVI and LAI over forests and savannas in the region 0°–20°S and 80°–40°W. Valid EVI and NDVI values are averaged over all forest pixels showing statistically significant green-up from June to October for EVI (Figure 6a). Similarly, valid LAI values are averaged over all forest pixels showing statistically significant increase in LAI (Figure 6c). Mean EVI, NDVI and LAI for savannas are the mean values over all savanna pixels in the region. The dry season, July to September, is shaded.

Brando et al., 2010] over the Amazon forests (Figure 2). What does an increase in EVI mean? Spatiotemporal changes in EVI are proposed to characterize similar variations in vegetation greenness [*Huete et al.*, 2002]. But, greenness itself is a poorly defined property of vegetation, unlike leaf area, for example. Nevertheless, a corresponding increase in dry season gross primary production (GPP) inferred from flux tower measurements at two experimental sites in Amazon forests [*Huete et al.*, 2006] lends credibility to the idea of enhanced greening, possibly from flushing of new leaves, during the light-rich dry season.

[4] The same seasonal changes in spectral reflectances of Amazon forests have been interpreted as resulting from large seasonal changes in green leaf area, a gradual increase through the dry season and a corresponding decrease through the wet season [*Myneni et al.*, 2007] (Figure 2). Green leaf area per unit ground area, or leaf area index (LAI) for short, is a physical attribute of vegetation, and thus measurable, and can be used to mechanistically quantify the exchange of energy, mass and momentum between the surface and the boundary layer [*Dickinson*, 1983]. The inferred seasonal swings in LAI were hypothesized to result from net leaf flushing in the light-rich dry season and net leaf abscission in the light-poor wet season, a behavior that is consistent with earlier reports of sunlight as the dominant proximate cue for leaf flushing in tropical forests [*Wright and van Schaik*, 1994] and not inconsistent with observations of enhanced GPP [*Huete et al.*, 2006] and carbon uptake [*Carswell et al.*, 2002; *Saleska et al.*, 2003] during the dry season, relative to the wet season, as younger leaves tend to be more photosynthetically vigorous than epiphyll-infested older leaves with poor stomatal control, as long as these light-limited forests [*Nemani et al.*, 2003; *Würth et al.*, 2005; *Graham et al.*, 2003; *Schuur*, 2003] remain well hydrated through deep roots [*Nepstad et al.*, 1994].

[5] The idea that tropical forests flush new leaves in response to various cues, and most prominently to sunlight, is not new [e.g., *Wright and van Schaik*, 1994]. However, the idea that these evergreen forests display large seasonal changes in leaf area is new [*Myneni et al.*, 2007]. It has also been argued by *Myneni et al.* [2007] that a gradually increasing leaf area enhances the evapotranspiratory water vapor flux into the atmosphere during the dry season, which would facilitate convection and increase the probability of rainfall during the late dry season, factors that influence a transition to the wet season [*Li and Fu*, 2004; *Fu and Li*, 2004]. Field-based studies support these ideas through reports of enhanced leaf area: 5.5 to 6.5 [*Carswell et al.*, 2002], 3.32 to 4.25 [*Pinto-Junior et al.*, 2010], 8% increase [*Malhado et al.*, 2009], a small increase [*Negrón Juárez et al.*, 2009] but consistent with work of *Myneni et al.* [2007], and a moderate increase in LAI [*Doughty and Goulden*, 2008]. Besides, higher (on average 30%) evapotranspiration fluxes have been observed during the dry season [*Juárez et al.*, 2007, 2008].

[6] Nevertheless, changes in vegetation canopy spectral reflectances do not necessarily imply changes in LAI. Changes in leaf optical properties from the exchange of older leaves for newer ones during the dry season, without changes in total leaf area, can also result in observed changes in vegetation canopy spectral reflectances. In fact, this has been the argument in one recent study [*Doughty and Goulden*, 2008], which reported disagreement between the seasonal course of MODIS LAI and ground-measured LAI. This is inconsistent with other data from the same forest in the Amazon that shows considerable litterfall in the wet season [*Xiao et al.*, 2005]. A more recent detailed analysis of litterfall data from 81 sites across the forests of tropical South America actually shows a relationship between litterfall and rainfall seasonality, with some evidence of high levels of litterfall during the wet season, in addition to the dry season [*Chave et al.*, 2010]. Nevertheless, a sensitivity analysis with a simple radiative transfer model confirmed [*Doughty and Goulden*, 2008] that changes in canopy reflectances could be explained from changes in leaf optical properties [*Roberts et al.*, 1998] alone. These findings have additional support from another study [*Asner and Alencar*, 2010], which suggested that the higher NIR canopy reflectance during the dry season could be due to enhanced new leaf area at the top of the canopy, with overall canopy leaf area remaining unchanged, presumably through abscission of more numerous older leaves in the bottom reaches of the canopy. Neither of these studies provided valid explanation for the observed decrease in NIR canopy reflectance during the wet season (Figure 1), although aging and epiphylls are invoked by *Doughty and Goulden* [2008] in a manner that is inconsistent with observations of leaf demography [*Reich et al.*, 2004] and phenological behavior (see Introduction by *Myneni et al.* [2007]) in tropical forests.

[7] This brings us to the heart of the debate: are the observed seasonal changes in NIR reflectance of Amazon forests (Figure 1) due to changes in leaf area, or to changes in leaf optical properties, or both? The proposition that changes in forest canopy reflectances are due alone to changes in leaf optical properties, as argued by *Doughty and Goulden* [2008] and *Asner and Alencar* [2010] and recently discussed by *Brando et al.* [2010], does not acknowledge ground-based measurements of seasonal leaf area changes [*Asner et al.*, 2004; *Carswell et al.*, 2002; *Pinto-Junior et al.*, 2010; *Malhado et al.*, 2009; *Negrón Juárez et al.*, 2009; *Doughty and Goulden*, 2008] and litterfall [*Xiao et al.*, 2005; *Chave et al.*, 2010], and emerging evidence regarding the role Amazon forests play in the transition from dry to wet season [*Li and Fu*, 2004; *Fu and Li*, 2004; *Juárez et al.*, 2007, 2008], all of which support the interpretation proposed by *Myneni et al.* [2007]. On the other hand, the argument that only leaf area changes explain changes of forest canopy reflectance ignores the very obvious changes in leaf optical properties between younger and older leaves and between healthy and epiphyll infested leaves. A way to reconcile these divergent views is the goal of this research.

[8] The rest of this paper is organized as follows: data and methods are described in Sections 2 and 3, respectively. Results are presented in Section 4, followed by discussion in Section 5. Finally, conclusions are presented in Section 6.

2. Data

2.1. Satellite Vegetation Data

[9] The latest version of NASA land products, Collection 5 (C5) Enhanced Vegetation Index (EVI), Normalized Difference Vegetation Index (NDVI) and Leaf Area Index (LAI) and landcover data sets are used in this study.

2.1.1. Collection 5 (C5) Vegetation Indices (VI)

[10] These are satellite data based measurements of vegetation greenness produced by NASA using blue (BRF_{BLUE}, 459–479 nanometers (nm)), red (BRF_{RED}, 620–670 nm) and near-infrared (BRF_{NIR}, 842–876 nm) band surface reflectance data, called Bidirectional Reflectance Factor (*BRF*), from the MODIS instrument aboard the Terra and Aqua satellites [*NASA Land Processes Data Active Archive Center* (*LP DAAC*), 2010a; *Huete et al.*, 2002]. VIs consist of NDVI and EVI. NDVI (1) is a radiometric measure of photosynthetically active radiation absorbed by canopy chlorophyll, and therefore, is a good surrogate measure of the physiologically functioning surface greenness level in a region [*Myneni et al.*, 1995]. NDVI has been used in many studies of vegetation dynamics in the Amazon [e.g., *Asner et al.*, 2000; *Dessay et al.*, 2004; *Ferreira and Huete*, 2004]. EVI (2) is also a measure of greenness that generally correlates well with ground measurements of photosynthesis [e.g., *Rahman et al.*, 2005; *Sims et al.*, 2008] and found to be especially useful in high biomass tropical broadleaf forests like the Amazon [*Huete et al.*, 2006]. C5 MODIS Terra VI data were used in this study.

$$NDVI = \frac{BRF_{NIR} - BRF_{RED}}{BRF_{NIR} + BRF_{RED}} \quad (1)$$

$$EVI = 2.5\frac{BRF_{NIR} - BRF_{RED}}{1 + BRF_{NIR} + 6BRF_{RED} - 7.5BRF_{BLUE}} \quad (2)$$

Two kinds of VI data sets were used, 1×1 km^2 and 16-day MOD13A2, and $0.05° \times 0.05°$ and 16-day MOD13C1, for the period February 2000–December 2009. The data set "Vegetation Indices 16-Day L3 Global 1 km" (MOD13A2) contains EVI (NDVI) at 1×1 km^2 spatial resolution and 16-day frequency. This 16-day frequency arises from compositing, i.e., assigning one best-quality EVI (NDVI) value to represent a 16-day period [*Huete et al.*, 2002]. This data set is available in tiles ($10° \times 10°$ at the equator) of Sinusoidal projection; 16 such tiles cover the Amazon region (approximately 10°N–20°S and 80°W–45°W). The data were obtained from the NASA Land Processes Data Active Archive Center (LP DAAC) (https://lpdaac.usgs.gov). The data set "Vegetation Indices 16-Day L3 Global 0.05Deg CMG" (MOD13C1) contains EVI (NDVI) at $0.05° \times 0.05°$ spatial resolution and 16-day frequency. These are "cloud-free spatial composites" of MOD13A2 [*LP DAAC*, 2010b].

2.1.2. Collection 5 (C5) Leaf Area Index (LAI)

[11] LAI is defined as the one-sided green leaf area per unit ground area in broadleaf canopies, and one-half the total surface area per unit ground area in needleleaf canopies (coniferous) [*Myneni et al.*, 2007]. LAI is operationally derived from atmospherically corrected surface reflectance in the red and NIR bands measured by the MODIS sensor onboard NASA's Terra and Aqua satellites [*LP DAAC*, 2010c]. The LAI retrieval algorithm ingests surface reflectances and their uncertainties, and information about land cover as well as sun and view geometry to estimate LAI from "look-up tables" (LUTs) pre-calculated using vegetation canopy radiative transfer model simulations [*Knyazikhin et al.*, 1998]. The C5 algorithm incorporates major improvements including an 8 biome input landcover map and refined LUTs, especially over woody biomes [*Shabanov et al.*, 2005]. The LAI product has been validated globally as well as at sites in the Amazon [*Yang et al.*, 2006; *Aragao et al.*, 2005], and has been used in studies of vegetation dynamics [e.g., *Myneni et al.*, 2007]. C5 MODIS Terra LAI data are used in this study.

[12] The data set "Leaf Area Index – Fraction of Photosynthetically Active Radiation 8-Day L4 Global 1 km" (MOD15A2) contains LAI at 1×1 km^2 spatial resolution and 8-day temporal frequency. This 8-day frequency arises from compositing, i.e., assigning one best-quality LAI value to represent an 8-day period. This data set is available in tiles ($10° \times 10°$ at the equator) of Sinusoidal projection; 16 such tiles cover the Amazon region (approximately 10°N–20°S and 80°W–45°W) [*LP DAAC*, 2010c]. The data were obtained from the NASA LP DAAC (https://lpdaac.usgs.gov) for the period February 2000–December 2009.

2.1.3. Landcover Data

[13] Land cover information was obtained from the "MODIS Terra Land Cover Type Yearly L3 Global 1 km SIN Grid" product (MOD12Q1). This is the official NASA C5 land cover data set [*LP DAAC*, 2009; *Friedl et al.*, 2010]. It consists of five land cover classification schemes at 1×1 km^2 spatial resolution. The International Geosphere Biosphere Programme (IGBP) land cover classification scheme was used to identify forest pixels in the Amazon region.

2.2. Leaf Spectral Data

[14] Leaf albedo (reflectance + transmittance) data in NIR were obtained from two published studies on the effects of age and epiphyll cover on leaf spectra in the Amazon [*Roberts et al.*, 1998; *Toomey et al.*, 2009]. Epiphylls comprise a wide range of organisms-lichens, liverworts, fungi, algae and bacteria-that infest leaf surfaces in humid tropical forests [*Toomey et al.*, 2009]. Epiphylls coat the surface of leaves, which decreases light interception in both the photosynthetically active (PAR, 400–700 nm) and NIR spectral intervals [*Roberts et al.*, 1998; *Toomey et al.*, 2009]. The data are categorized into two classes, age-based and epiphyll-based. The age-based class consists of new and old leaves: new leaves are about 70 days in age (late dry season), fully formed and with minimal infestation while old leaves are a year old (late wet season/early dry season) and moderately infested. Spectra for this class are available for four plants of the Caatinga (low density scrubs, woodlands and woodland forests) dominant *Aldina heterophylla* [*Roberts et al.*, 1998]. The epiphyll-based class comprises clean and colonized leaves; clean leaves refer to mature leaves with no epiphyll infestation while colonized leaves refer to mature leaves that are moderately colonized by epiphyll. Spectra for this category are available for two Caatinga dominants, *Pradosia schomburgkiana* and *Protium heptaphyllam* [*Roberts et al.*, 1998], and three Terra Firme (dense forests) dominants, *Byrsonima* cf *poeppigiana*, *Inga* cf *sertulifera* and *Porouma tomentosa* [*Toomey et al.*, 2009]. The higher leaf albedo of new leaves is due to greater transmittance, while reflectance changes are minimal. The effect of epiphyll infestation is to reduce both reflectance and transmittance; relative decline in

transmittance is greater than reflectance [*Roberts et al.*, 1998; *Toomey et al.*, 2009].

3. Methods

3.1. VI Data Quality

[15] The quality of VI (EVI/NDVI) data in each pixel can be assessed using the accompanying 16-bit quality flags, in both 1×1 km^2 as well as the $0.05° \times 0.05°$ products. Sets of bits, from these 16 bits, are assigned to flags pertaining to clouds and aerosols (details can be found in work by *Samanta et al.* [2010, 2011a, 2011b] and *Xu et al.* [2011]). Each 1×1 km^2 16-day composite VI value is considered valid when (a) VI data is produced—"MODLAND_QA" equals 0 (good quality) or 1 (check other QA), (b) VI Usefulness is between 0 and 11, (c) Clouds are absent—"Adjacent cloud detected" (0), "Mixed Clouds" (0) and "Possible shadow" (0), and (d) Aerosol content is low or average—"Aerosol Quantity" (1 or 2). Note that "MODLAND_QA" checks whether VI is produced or not, and if produced, its quality is good or whether other quality flags should also be checked. Besides, VI Usefulness Indices between 0 to 11 essentially include all VI data. Thus, these two conditions serve as additional checks. Each $0.05° \times 0.05°$ 16-day VI pixel is considered valid when (a) VI data is produced—"MODLAND_QA" equals 0 (good quality) or 1 (check other QA), (b) VI Usefulness is between 0 and 11, (c) Clouds are absent—"Adjacent cloud detected" (0) and "Mixed Clouds" (0), and (d) Aerosol content is low or average—"Aerosol Quantity" (1 or 2). Here, the utility of "MODLAND_QA" and VI Usefulness flags is the same as in the case of 1×1 km^2 VI validity.

3.2. LAI Data Quality

[16] The quality of LAI data in each 1×1 km^2 8-day pixel can be assessed using two accompanying 8-bit quality flags, FparLai_QC and FparExtra_QC (details can be found in work by *Samanta et al.* [2011b]). The validity of LAI was determined through a two-stage process: (1) a 1×1 km^2 8-day LAI pixel was considered valid when (a) data is of good quality—"SCF_QC" equals 0 (main algorithm without saturation) or 1 (main algorithm with saturation), (b) Clouds are absent—"CloudState" (0), "Cirrus" (0), "MODAGAGG_Internal_CloudMask" (0) and "MODAGAGG_Cloud_Shadow" (0). (2) As the 8-day LAI aerosol flag does not distinguish between average and high aerosol loadings nor reports climatology aerosols, valid 8-day values are averaged to 16-day LAI whose validity was further determined using MOD13A2 cloud and aerosol flags: (a) VI data is produced-"MODLAND_QA" equals 0 (good quality) or 1 (check other QA), (b) VI Usefulness is between 0 and 11, (c) Clouds are absent—"Adjacent cloud detected" (0), "Mixed Clouds" (0) and "Possible shadow" (0), and (d) Aerosol content is low or average-"Aerosol Quantity" (1 or 2). Valid 1×1 km^2 16-day values were averaged to obtain monthly LAI. Finally, valid 1×1 km^2 monthly LAI values are aggregated to 8×8 km^2 spatial resolution. This 8×8 km^2 monthly LAI data set spanning February 2000–December 2009 was used in this study.

[17] In order to test the effectiveness of the quality flags, we have analyzed the seasonal time series of surface reflectances and vegetation indices (VI) of both uncorrupted (clean) and corrupted (contaminated) data (Figure S1). Interaction of photons with dense Amazonian forests is characterized by strong scattering in near-infrared (NIR), and equally strong absorption in the shorter red and blue wavelengths. The NIR reflectance of these forests is an order of magnitude greater than the reflectance at red (blue) wavelengths. On the other hand, atmospheric influences scatter more strongly in the shorter red/blue wavelengths. Thus, NIR reflectance is much less affected by atmospheric effects in comparison to red (blue) reflectance, which is shown in Figure S1a. Contaminated red reflectances are artificially higher-almost double in magnitude in comparison to clean values (Figure S1a). The difference between clean and contaminated red reflectance remains steady during the course of the year, which indicates lack of bias due to seasonal changes in atmospheric effects, such as high aerosol loads in the dry season from biomass burning (e.g., as discussed by *Samanta et al.* [2010]). These changes in surface reflectances translate into lower estimates of surface greenness or VIs. NDVI reduces by about 24% and EVI by about 18%, especially during the dry season (Figure S1b). Moreover, *Myneni et al.* [2007] have reported that residual atmospheric effects reduce leaf area index (LAI) estimates by about 5% during the dry season. These results show that seasonal variations in atmosphere-corrupted data are inconsistent with those observed with clean data. Furthermore, any remaining residual atmospheric influences that would reduce seasonal changes in measured greenness are eliminated by ensuring that the observed increase in VIs is greater than the errors in VIs (as mentioned in the caption of Figure 6). Thus, we conclude that the seasonal changes in vegetation greenness reported in the manuscript are not an artifact of residual atmospheric effects in surface reflectances.

3.3. Saturation of NDVI

[18] Photosynthesizing (green) vegetation strongly absorbs in red and blue bands and scatters in the NIR band. NIR reflectance of dense canopies such as Amazonian forests is an order of magnitude higher than red reflectance (Figures 1 and S1). In such situations, the formulation of NDVI (1) renders it relatively insensitive to changes in NIR, which can be shown as follows:

$$\delta NDVI = \frac{2BRF_{RED}}{(BRF_{NIR}+BRF_{RED})^2}\delta BRF_{NIR} - \frac{2BRF_{NIR}}{(BRF_{NIR}+BRF_{RED})^2}\delta BRF_{RED}$$

$$\delta NDVI = \frac{2BRF_{RED}}{(BRF_{NIR}+BRF_{RED})^2}\delta BRF_{NIR}, \delta BRF_{NIR} \gg \delta BRF_{RED}$$

$$\frac{\delta NDVI}{NDVI} = 0.2\frac{\delta BRF_{NIR}}{BRF_{NIR}}, BRF_{NIR} \sim 10BRF_{RED} \quad (3)$$

Similarly, for EVI we can write,

$$\delta EVI = G\frac{(1+C1)BRF_{RED} - C2BRF_{BLUE} + L}{(BRF_{NIR} + C1BRF_{RED} - C2BRF_{BLUE} + 1)^2}\delta BRF_{NIR},$$

$$\delta BRF_{NIR} \gg \delta BRF_{RED}, \delta BRF_{BLUE}$$

$$\frac{\delta EVI}{EVI} = \left(\frac{\delta BRF_{NIR}}{BRF_{NIR}}\right)\left[\frac{1+0.325BRF_{NIR}}{0.9(1+1.225BRF_{NIR})}\right],$$

$$C1 = 6, C2 = 7.5, BRF_{NIR} \sim 10BRF_{RED}, BRF_{RED} \sim 2BRF_{BLUE} \quad (4)$$

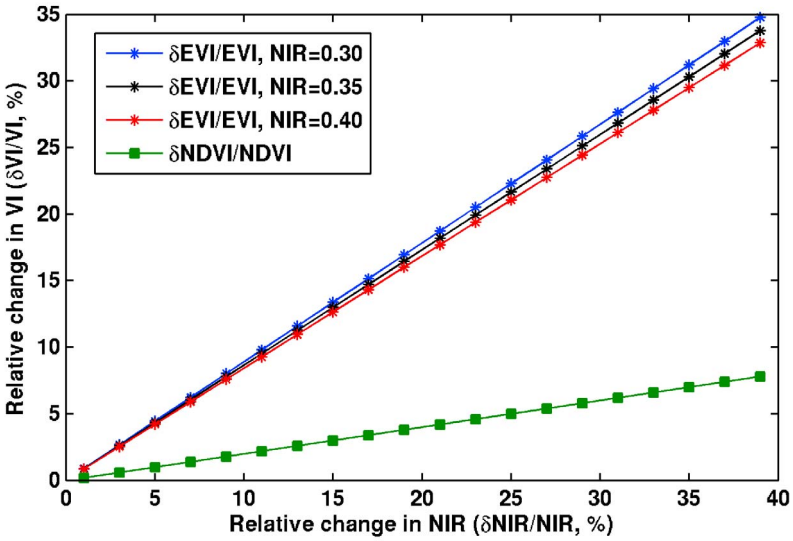

Figure 3. Sensitivity of Enhanced Vegetation Index (EVI) and Normalized Difference Vegetation Index (NDVI) to changes in near-infrared (NIR) reflectance (BRF_{NIR}) for dense vegetation. NIR reflectance is set at 10*red (BRF_{RED}) and 20*blue (BRF_{BLUE}), which is typically observed in dense canopies such as Amazon forests. Note that relative change in NDVI is independent of the magnitude of NIR reflectance.

Equation (4) implies that a given increase in NIR would translate into a five times lesser increase in NDVI (Figure 3). On the other hand, EVI is very sensitive to changes in NIR and does not exhibit the saturation problem (Figure 3).

3.4. Sensitivity of BRF to Variation in LAI and Leaf Optics

[19] The theory of spectral invariants [*Knyazikhin et al.*, 2010] was used to examine the sensitivity of the canopy near-infrared (NIR) *BRF* to LAI and leaf optical properties under saturation conditions. If the impact of canopy background on canopy reflectance is negligible as in the case of dense Amazonian forests, the spectral *BRF* can be approximated as [*Knyazikhin et al.*, 2010; *Schull et al.*, 2010; *Huang et al.*, 2008]:

$$BRF(\lambda,\Omega)=\frac{\rho(\Omega)\omega_\lambda}{1-p\omega_\lambda}i_0=\left[\frac{\rho(\Omega)}{1-p}i_0(\Omega_0)\right]\left[\frac{\omega_\lambda(1-p)}{1-p\omega_\lambda}\right]=K(\Omega,\Omega_0)W_\lambda \tag{5}$$

Here ρ is the directional escape probability, i.e., probability that a photon scattered by a leaf will escape the vegetation medium in a given direction Ω. It also can be interpreted as the probability of seeing a gap in the direction Ω from a leaf surface [*Stenberg*, 2007]. Spherical integration of ρ over all directions gives the total escape probability, $(1-p)$, where p is the recollision probability, i.e., the probability that a photon scattered by a leaf will interact with another leaf in the canopy again. Further, i_0, the probability of initial collision, or canopy interceptance, is the portion of incoming photons that collide with leaves for the first time. It depends on the direction of radiation incident on the vegetation canopy. Finally, ω_λ is the leaf albedo, which is the portion of the radiation incident on the surface of an individual leaf that the leaf transmits or reflects. In the present approach, this is the only variable that is dependent on the wavelength. It allows the parameterization of *BRF* in terms of leaf albedo rather than wavelength. Therefore wavelength dependence will be suppressed in further notations.

[20] Two separate factors are shown in equation (5), each exhibiting a different sensitivity to canopy structure and leaf optics. The wavelength independent ratio $P = \rho/(1 - p)$ gives the portion of gaps as seen from a leaf surface in a given direction Ω. This variable is sensitive to canopy geometrical properties such as spatial distribution of trees, ground cover, crown shape, size, and transparency [*Schull et al.*, 2010]. In the case of Amazon forests, changes in canopy structure over monthly time-scales are assumed negligible. At high LAI values, the canopy interceptance i_0 varies insignificantly with LAI due to the saturation. Under such conditions, the observed variation in NIR *BRF* is much stronger than corresponding variation in $K = Pi_0$, typically 2–3%, and thus changes in canopy structure alone cannot explain the observations (cf. Section 3.4.1).

[21] The second factor is the canopy scattering coefficient, $W_\lambda = \omega_\lambda\ (1 - p)\ /\ (1 - p\omega_\lambda)$ [*Smolander and Stenberg*, 2005], which depends on both canopy structure and leaf optics. It increases with the leaf albedo; the more the leaves scatter, the brighter the canopy is. Variations in LAI, however, trigger an opposite tendency. As the recollision probability increases with LAI [*Knyazikhin et al.*, 1998; *Smolander and Stenberg*, 2005; *Rautiainen et al.*, 2009], an increase in LAI results in more photon-canopy interactions and consequently a higher chance for photon to be absorbed. This mechanism makes the canopy appear darker. The effect of multiple scattering is described by the denominator in the equation for W_λ [*Huang et al.*, 2008], which in turn is fully determined by the product $\kappa = p\omega_\lambda$. An increase in κ not only enhances the effect of multiple scattering but also changes the sensitivity of the *BRF*: the closer its value is to unity, the stronger the response of canopy *BRF* to variations in canopy structure and leaf optics. If variation in K is negligible, changes in *BRF* can be reduced to examining variations in the scattering coefficient.

[22] The vegetation canopy is parameterized in terms of the recollision probability, $0 \le p \le 1$, leaf albedo, $0 \le \omega \le 1$, and the sensitivity parameter, $\kappa = p\omega \le \min(\omega, p)$. Let the sensitivity of *BRF* to canopy structure and leaf optics at time t and $t_1 = t + \Delta t$ be κ and $\kappa_1 = \kappa + \delta\kappa$, $\delta\kappa \ge 0$, respectively. Note that κ and κ_1 do not uniquely specify the recollision probabilities and leaf albedos since various combinations can result in the same values of the sensitivity parameter, which impact canopy reflective properties differently. To characterize the contribution of LAI to a change in the sensitivity parameter from by κ to $\kappa+\delta\kappa$, the following impact function is introduced:

$$k = \frac{\delta p/p}{\delta\kappa/\kappa} = \frac{\delta p/p}{\delta p/p + \delta\omega/\omega} \tag{6}$$

In general, k varies between $-\infty$ and $+\infty$. Values of k greater than 1 imply a decrease in leaf albedo, i.e., $\delta\omega/\omega < 0$. Variations in LAI and leaf optics make the vegetation darker in this case. On the other hand, a decrease in canopy structure, $\delta p/p < 0$, involves a negative value of the parameter k. In this case, changes in p and ω lead to brightening of the vegetated surface. This study will focus on the case when both LAI and leaf albedo increase, i.e., k varies between 0 (no change in LAI) and 1 (no change in leaf albedo). Such variations trigger competing processes: changes in LAI tend to darken the vegetation while variations in the leaf albedo suppress it. It should be emphasized, however, that this mechanism refers to the scattering coefficient W_λ and is applicable to $BRF = KW_\lambda$ (cf. equation (5)) if variations in K are negligible. In general, K increases with LAI and therefore compensates for a decrease in the canopy scattering coefficient. This lowers the darkening effect and even can result in an increase in the canopy *BRF* (cf. Sections 3.4.2 and 3.4.3).

[23] Under saturation conditions (i.e., $\delta BRF/BRF \gg \delta K/K$), the impact function ($k$), sensitivity parameter (κ), leaf albedo at time t (ω), variations $\delta BRF/BRF$, $\delta K/K$ and $\delta\kappa/\kappa$ are related as (cf. Section 3.4.1):

$$k(\omega) = \frac{\omega - \kappa}{\omega}\theta \tag{7}$$

where

$$\theta = \frac{1}{1-\kappa} - \beta, \beta = \frac{\delta BRF/BRF - \delta K/K}{\delta\kappa/\kappa} \tag{7a}$$

Here β characterizes the amplitude of the variability in reflectance. Since the goal of this study is to examine contributions of LAI and leaf albedo to large positive changes in the canopy *BRF* under saturation conditions, i.e., $\delta BRF/BRF \gg \delta K/K$, this analysis is restricted to the case when $\beta > 0$. It should be noted that in general, $\delta K/K$ is proportional to the impact function k (cf. Section 3.4.1). Under saturation conditions, this term can be neglected, and thus, equation (7) quantifies the impact of canopy structure on the *BRF* when both LAI and ω vary.

[24] If $k(\omega) = 1$ ($\delta\kappa/\kappa = \delta p/p$), then $(\omega-\kappa)\theta/\omega = 1$. This relationship holds true if and only if $\beta \le 0$ (cf. Section 3.4.1). It means that LAI alone cannot explain positive changes in canopy *BRF* under the saturation condition.

[25] If $k(\omega) = 0$ ($\delta\kappa/\kappa = \delta\omega/\omega$), then either $\omega = \kappa$ or $\theta = 0$. The former corresponds to an extreme and unrealistic case when $p = 1$. It means that photons cannot escape the vegetation canopy and therefore $BRF = 0$. The latter implies that variations in canopy *BRF* are proportional to $\delta\omega/\omega$, i.e.,

$$\frac{\delta BRF}{BRF} = \frac{1}{1-\kappa}\frac{\delta\omega}{\omega} \tag{8}$$

One can see that the closer the value of the sensitivity parameter is to unity, the stronger the response of the *BRF* to leaf albedo. Changes in leaf optics alone can explain a rather large range of variation in canopy reflectance under the saturation conditions.

[26] If $0 < k(\omega) < 1$ (i.e., $\delta p/p > 0$ and $\delta\omega/\omega > 0$), the contribution of LAI to the *BRF* is given by equation (7). It should be emphasized that this equation refers to the case when both LAI and the leaf albedo are changing. Figure 4 illustrates the LAI versus leaf albedo "competing process" under saturation conditions, which results in the observed *BRF* change by 23% ($\delta BRF/BRF = 0.23$ and $\delta BRF/BRF \gg \delta K/K = 0.01$, cf. Sections 3.4.2 and 3.4.3).

3.4.1. Derivation of Equation (7)

[27] It follows from equation (5) that

$$\frac{\delta BRF}{BRF} = \delta \ln BRF = \frac{\delta K}{K} + \frac{1}{1-p\omega}\left[\frac{\delta\omega}{\omega} - \frac{p(1-\omega)}{1-p}\frac{\delta p}{p}\right] \tag{9}$$

We parameterize the relative variation in *BRF* in terms of the sensitivity parameter, κ, its variation, $\delta\kappa/\kappa$, and the impact function, k, by substituting $p = \kappa/\omega$, $\delta p/p = k\delta\kappa/\kappa$ and $\delta\omega/\omega = (1-k)\delta\kappa/\kappa$ into equation (9). Solving the resulting equation for k yields equation (7).

[28] Case $k(\omega) = 1$: Letting $\delta\omega/\omega = 0$ in equation (9) and taking into account that $p(1-\omega)/(1-p\omega)(1-p)$ decreases with ω, one gets

$$-\frac{\delta p}{1-p} \le \frac{\delta BRF}{BRF} - \frac{\delta K}{K} \le 0 \tag{10}$$

Thus, a positive response of *BRF* to a positive variation in the recollision probability can be achieved if the parameter β defined by equation (7a) is negative.

3.4.2. Assumptions

[29] Since our goal is the qualitative description of the sensitivity of *BRF* to LAI and leaf albedo under the saturation conditions, we use a simple canopy model to specify the relationship between $\delta p/p$, δLAI/LAI and $\delta K/K$. We idealize the vegetation canopy as a spatially homogeneous layer filled with small planar elements of infinitesimally small sizes. All organs other than green leaves are ignored. For such a structurally simple uniform canopy, *Stenberg* [2007] found an analytical formula that relates the recollision probability, p, and canopy interceptance, $i_{0,d}$, under diffuse illumination condition, i.e.,

$$i_{0,d} = (1-p)LAI \tag{11}$$

Analyses of LAI-2000 data suggest the following relationship between $i_{0,d}$ and *LAI* [*Rautiainen et al.*, 2009]

$$i_{0,d} = 1 - \exp(-k_{CAN} \cdot LAI) \tag{12}$$

where the coefficient $k_{CAN} = 0.81$ was found to be almost insensitive to stand age, tree species or growing conditions. Finally, the canopy interceptance, i_0, can be estimated as $i_0 = 1 - \exp(-G \cdot \mathrm{LAI}/\mu_0)$ where G and μ_0 are the geometry

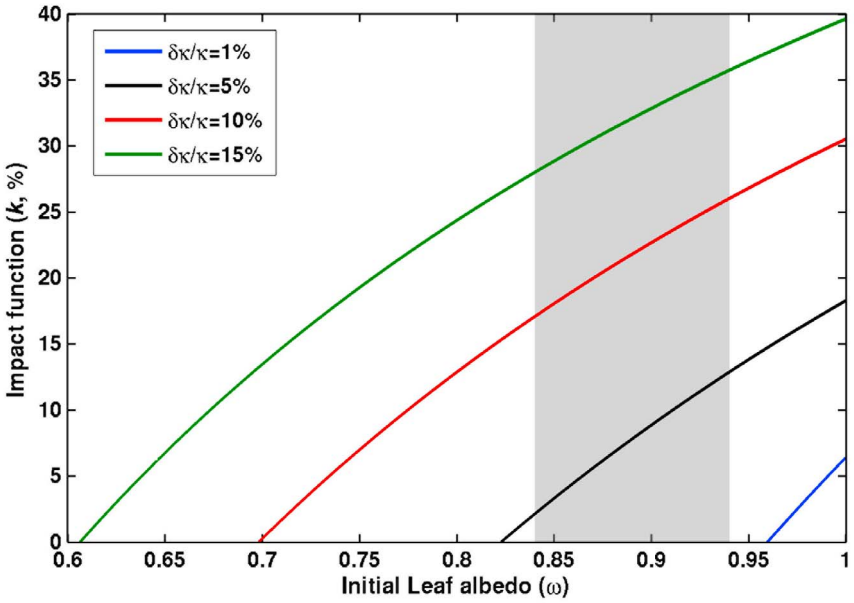

Figure 4. Impact function k (%) for a 23% increase in canopy near-infrared (NIR) bi-directional reflectance factor (*BRF*) and three values of the sensitivity parameter, $\kappa = 0.6$, 0.7, 0.82 and 0.96. The horizontal axis represents the initial value (late wet season/early dry season, June) of the leaf albedo ω, i.e., $\omega p = \kappa$. Each line corresponds to a fixed change in the sensitivity parameter from κ to $\kappa + \delta\kappa/\kappa$ and crosses the horizontal axis at the corresponding sensitivity parameter κ. Vertical axis shows the relative contribution of the recollision probability p to the 23% change in the NIR *BRF*. For example, if $\omega = 0.9$, a value of the recollision probability corresponding to $\kappa = 0.7$ is 0.7/0.9 = 0.78. For this combination of $p = 0.78$ and $\omega = 0.9$, the 23% change in *BRF* is attainable from changes in the recollision probability and leaf albedo by $k(0.9)\delta\kappa/\kappa = 0.23 \times 0.10 = 2.3\%$ (red curve) and $(1-k(0.9))\delta\kappa/\kappa = 0.77 \times 0.10 = 7.7\%$, respectively. The 2.3% change in $p = 0.78$ translates to an 11% increase in LAI of 4.5. The shaded region shows the range of initial NIR leaf albedo values (late wet season/early dry season, and leaves that are old and/or epiphyll infested) from field-based studies in the Amazon (cf. Section 2.2).

factor [*Ross*, 1981] and cosine of the solar zenith angle (SZA), respectively. It follows from this equation and equation (11) that

$$1 - i_0 = \left(1 - i_{0,d}\right)^{\alpha} \tag{13}$$

where $\alpha = G/(k_{CAN}\mu_0)$. For simplicity, the geometry factor G is set to $k_{CAN}\mu_0 = 0.81*\cos(30) = 0.81*0.87 = 0.70$ (mean SZA = 30°, std. = 5°–6° (20%)). The mean SZA for the dry season is about 30° and varies by about 5°–6° during this time, as reported in the MODIS VI data. Therefore, the small changes in SZA are not likely to induce large changes in μ_0, and G. Under the above assumptions, LAI is the only variable that fully describes canopy structure. The recollision probability (p) is an increasing function of LAI.

[30] We neglect angular dependence of the directional escape probability by replacing this term by its hemispherically integrated counterpart, i.e., $\rho(\Omega) = r/\pi$ where r is the probability that a scattered photon will escape the vegetation canopy through its upper boundary. Neglecting radiation transmitted through a very dense canopy, we get $\rho(\Omega) = (1 - p)/\pi$. The relative portion of gaps as seen from a leaf surface, $P = \rho/(1 - p)$, is approximated by a constant and thus $\delta K/K = \delta P/P + \delta i_0/i_0 \approx \delta i_0/i_0$. Note that this approximation is accurate for the uniform canopies with horizontally oriented leaves since such canopies transmit and reflect radiation diffusely and approximate for other canopies.

3.4.3. Properties of the Impact Function

[31] The impact function k requires specification of the parameter θ, which includes the term $\delta BRF/BRF - \delta K/K$ that appears in β. Our structurally simple canopy suggests negligible contribution of $\delta K/K \approx \delta i_0/i_0$ under the saturation conditions. For example, a change in LAI from 5 to 6 results in $\delta i_0/i_0 \approx 1\%$ which is significantly below the observed variation, $\delta BRF/BRF \approx 23\%$, in NIR surface reflectance. Although a more realistic canopy model can result in a different value of the relative variation in K, its use would not change our qualitative results as long as $\delta BRF/BRF \gg \delta K/K$. Figure 5 and the following properties of the impact function provide the necessary justification.

[32] If $\theta \geq 0$, the impact function k has the following properties (Figure 5).

$$\text{A. } \lim_{\omega \to 0+} k(\omega) = -\infty;$$

$$\text{B. } k(\kappa) = 0;$$

$$\text{C. } \lim_{\omega \to \infty} k(\omega) = \theta = \frac{1}{1-\kappa} - \beta;$$

[33] D. *If* $\theta > 1$, the equation $k(\omega) = 1$ has a unique solution given by $\omega^* = \kappa\psi$ where

$$\psi(\beta, \kappa) = \frac{\theta}{\theta - 1} = \frac{1 - \beta(1-\kappa)}{\kappa - \beta(1-\kappa)} = \frac{1}{\kappa} \quad \frac{1 - \beta(1-\kappa)}{1 - \beta\frac{1-\kappa}{\kappa}}$$

The function ψ increases with β and decreases with κ.

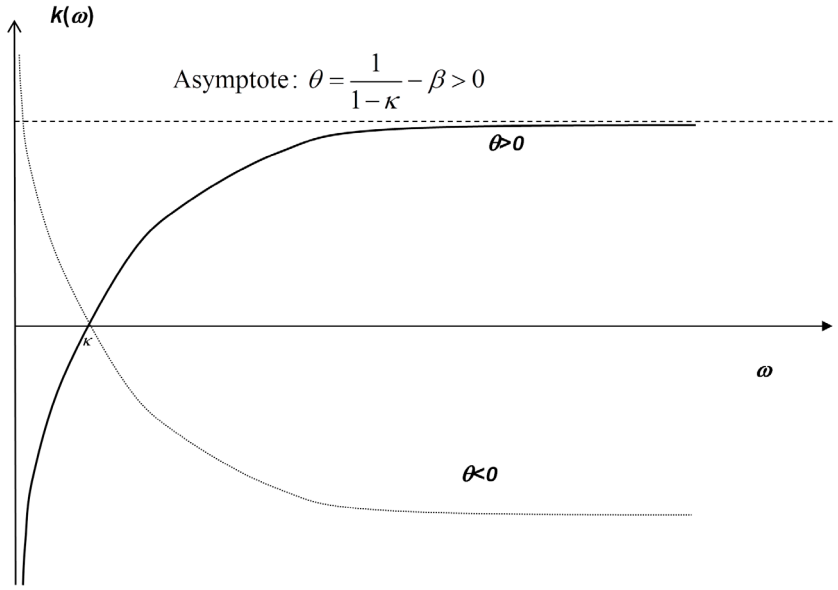

Figure 5. Schematics of properties A–C of the impact function $k(\omega)$. For positive θ, interpretation of $\delta BRF/BRF$ depends on the location of the asymptote relative to unity, i.e., whether $\theta \leq 1$ or $\theta > 1$ (i.e., property D described in Section 3.4.1).

[34] If $\theta \leq 0$, its properties can be formulated in a similar manner (see Figure 5). Let $\theta > 0$, i.e., $\beta < 1/(1 - \kappa)$. As one can see from Figure 5, interpretation of variation in the *BRF* depends on the location of the asymptote and the root of the equation $k(\omega) = 1$ relative to unity. The following cases are possible.

[35] Case 1: $0 < \theta < 1$, i.e., $\beta > \kappa/(1 - \kappa)$. The asymptote is below unity. If $\omega \leq \kappa$, the impact of canopy structure is negative (i.e., LAI should decrease in order to achieve a given variation in *BRF*). If $\omega > \kappa$, both the canopy structure and leaf optics have a positive impact. If θ tends to zero, the impact of canopy structure becomes negligible.

[36] Case 2: $\theta \geq 1$, i.e., $\beta \leq \kappa/(1 - \kappa)$. The asymptote is above unity. The equation $k(\omega) = 1$ has a solution given by $\omega^* = \kappa\psi$. Since ψ increases with β, the solution is above unity if $\beta > 0$; is equal to 1 if $\beta = 0$ and approaches to κ if β tends to $-\infty$. If κ tends to unity, the solution tends to unity, resulting in a jump from $k = 0$ to 1 at $\omega = \kappa$. Thus, if $\omega \leq \kappa$, the impact of canopy structure is negative. If $\kappa < \omega \leq \omega^*$, both structure and leaf optics positively contribute to variation in *BRF*. If $\omega > \omega^*$, the impact of structure is positive and leaf optics is negative.

[37] To summarize, a small variation in the parameter β does not change qualitatively the behavior of the impact function. Under saturation conditions, i.e., $\delta BRF/BRF \gg \delta K/K$, and the term $\delta K/K$ can be neglected.

4. Results

4.1. Comparison of Dry-Season Greening Patterns With Previous Studies

[38] Nearly 48% of Amazon forests (forests south of the Equator) display statistically significant EVI increase of about 16% from June to October in a given year during 2000–2009, which is in contrast to about 22% decline in EVI over the adjoining savannas from June to September (Figures 6a and 2). Approximately opposing changes are observed over these two vegetation types during the wet season (Figure 2). Interestingly, NDVI data do not show any appreciable changes in forests during the dry season (Figure 6b), or during other times of the year (Figure 2). However, the same data display large swings over savannas consisting of decline during the dry season and increase during the wet season, with an amplitude of about 41% (Figure 2). Further, LAI increase of about 0.93 units (18%) is observed over 33% of Amazon forests, while LAI decline of about 1.1 units is observed over adjacent Savannas during the dry season (Figures 6c and 2). These LAI variations are part of a seasonal cycle of opposing timing between forests and savannas (Figure 2). Thus, MODIS EVI and LAI data show large seasonal variations of approximately opposing timing over forests and savannas, with green-up of 16–18% over a third to half of Amazon forests during dry seasons of the decade 2000–2009.

[39] The spatial patterns of dry-season EVI increase seen here (Figure 6a) are consistent with a previous report [*Huete et al.*, 2006], albeit the magnitude of forest green-up is smaller (16% versus 25%) and is similar over a broad region extending across a large gradient in number of dry seasons, from the perpetually wet northwestern parts to the seasonally dry southeastern parts of the Amazon basin. Besides, the elimination of atmosphere-corrupted data (persistent during the dry season [e.g., *Samanta et al.*, 2010]) results in missing patches, especially in eastern Amazonia (Figures 6a and 6b). While the spatial patterns of dry-season enhancement in LAI (Figure 6c) are similar to those in work by *Myneni et al.* [2007], the extent (33% versus 68%) and average magnitude (0.93 versus 1.2) of LAI upswing are smaller than the previous estimate. These changes are attributable to the improved C5 LAI algorithm [*Shabanov et al.*, 2005] and

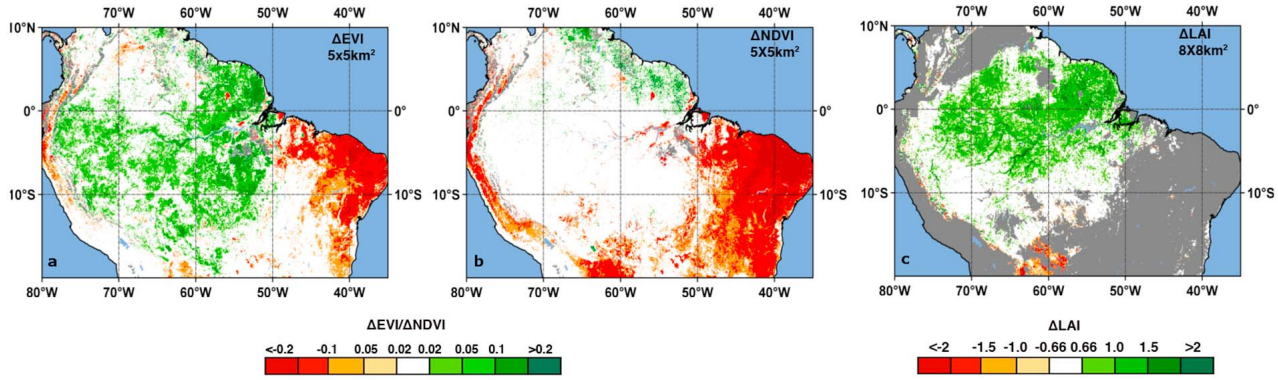

Figure 6. Spatial patterns of dry season greenness changes in the Amazon. (a) Change in Enhanced Vegetation Index (EVI), at 0.05° × 0.05° spatial resolution, from June (EVI_{jun}) to October (EVI_{oct}) expressed as ΔEVI (EVI_{oct} - EVI_{jun}) as in work by *Huete et al.* [2006]. Shown are only statistically significant changes i.e., $|\Delta EVI| >= |0.04*EVI_{jun} + 0.04|$ (2 standard deviation or 95% confidence interval of error in EVI_{jun} [*Vermote and Kotchenova*, 2008]). (b) Same as Figure 6a but for Normalized Difference Vegetation Index (NDVI). (c) Change in Leaf area index (LAI), at 8 × 8 km^2 spatial resolution, greater than 0.66 or less than −0.66. This threshold (|0.66|) is the smallest LAI difference discernable with the MODIS LAI data set. The amplitude, in regions with dry seasons longer than three months, is calculated as the difference between the maximum four-month average LAI in the dry season minus the minimum four-month average LAI in the wet season. Where the dry season is three or fewer months, the amplitude is calculated as the difference between the dry season average LAI and the minimum four-month average LAI in the wet season. The definition of the dry season is the same as in work by *Myneni et al.* [2007]. LAI difference for only forest pixels is shown as by *Myneni et al.* [2007]. Missing data are also shaded white.

with stricter screening of cloud-and aerosol-corrupted data. The patterns of seasonal greenness changes of Amazon forests observed with the latest version (C5) of MODIS greenness data are generally similar to previous reports.

4.2. Plausible Mechanisms of Dry-Season Increase in NIR Reflectance

[40] The cause of dry season increase in NIR BRF of Amazon forests (Figure 1) can be ascertained by assessing its sensitivity to LAI and leaf albedo (see Section 3.4; in this section, the term *BRF* is used instead of the more colloquial term, reflectance, to be technically consistent with the formulation in Section 3.4). This is determined by the sensitivity parameter ($\kappa = p\omega$), which couples vegetation canopy structure p (a function of LAI) and leaf albedo, ω. Positive changes in p and ω lead to an increase in the sensitivity parameter κ, which in turn alters how the *BRF* responds to changes in canopy structure and leaf optics. An increase in canopy *BRF* can be due to changes in (*i*) the sensitivity parameter from κ to $\kappa_1 = \kappa + \delta\kappa$ and (*ii*) canopy structure from p to $p_1 = p + \delta p$ and leaf optics from ω to $\omega_1 = \omega + \delta\omega$ such that $\kappa_1 = p_1\omega_1$ (cf. Section 3.4). The observed dry season increase in NIR *BRF* can be achieved variously, as discussed below.

4.2.1. Increase in LAI and Leaf Albedo Unchanged

[41] In this case, $\delta p/p > 0$ and $\delta\omega/\omega = 0$, i.e., $k = 100\%$ and $\delta\kappa/\kappa = \delta p/p$ (see Section 3.4). Variation in *BRF* does not exceed variation in K (see equation (5)), resulting in a negative value of the parameter β (cf. Section 3.4.1). In other words, adding more leaf area with the same spectral properties as the rest of the canopy will not change the observed canopy reflectance. Thus, the observed change in NIR *BRF* cannot be achieved by only increasing LAI.

4.2.2. Increase in Leaf Albedo and LAI Unchanged

[42] In this case, $\delta p/p = 0$ and $\delta\omega/\omega > 0$, i.e., $k = 0$ and $\delta\kappa/\kappa = \delta\omega/\omega$ (see Section 3.4). The relationship between variation in *BRF* and leaf albedo is given by (equation (8)), which suggests a strong response of the *BRF* to variation in leaf albedo. This response becomes stronger as the sensitivity parameter approaches unity, which is typical of dense vegetation and leaf albedo at NIR wavelengths. For instance, the observed 23% increase in NIR *BRF* can be attained through an increase in ω by $\delta\omega/\omega = 6.9\%$ for $\kappa = 0.7$ and any combination of ω and p such that $\omega p = \kappa = 0.7$. In the case of Amazonian forests, possible combinations could be $\omega = 0.9$ and $p = 0.78$ (which corresponds to LAI = 4.5), or $\omega = 0.88$ and $p = 0.8$ (LAI = 5). Thus, variations in leaf optics alone can explain the observed *BRF* changes, consistent with the arguments by *Doughty and Goulden* [2008], *Asner and Alencar* [2010], and *Brando et al.* [2010].

4.2.3. Increase in Both LAI and Leaf Albedo

[43] In this case, $\delta p/p > 0$ and $\delta\omega/\omega > 0$, i.e., $0 < k < 100\%$ and $\delta\kappa/\kappa = \delta\omega/\omega + \delta p/p$ (see Section 3.4). Changes in leaf optics and LAI that can lead to the observed dry season variation in *BRF* depend on the sensitivity parameter κ and its increment $\delta\kappa$. This is illustrated in Figure 4. For instance, consider a 10% change in the *BRF* sensitivity from $\kappa = 0.7$ (in early dry season, June) to $\kappa_1 = 0.77$ (in late dry season, September/October) ($\delta\kappa/\kappa = 0.10$). This case is described by the red curve in Figure 4. Assuming $\omega = 0.9$ in June (horizontal axis in Figure 4), the impact of canopy structure to *BRF* change is $k(0.9) = 23\%$ (vertical axis in Figure 4). It means that the 23% increase in NIR *BRF* would require an

increase in p of 2.3% ($k(0.9)$, $\delta\kappa/\kappa = 0.23 \times 0.10 = 2.3\%$; $p = \kappa/\omega = 0.78$ in June to $p_1 = 0.80$ in September/October) which translates into an 11% increase in LAI of 4.5. The corresponding increase in leaf albedo is 7.7% [$(1 - k(0.9))\delta\kappa/\kappa = 0.77 \times 0.10$]. In this example, a larger increment of the leaf albedo is required to achieve a given increase in *BRF* compared to the previous case of $\kappa = 0.7$ and unchanged LAI ($\delta\omega/\omega = 6.9\%$). Thus, variation in both leaf optics and LAI can equally well explain the observed *BRF* change, not inconsistent with *Myneni et al.* [2007], who interpreted the increased NIR *BRF* as more leaf area during the dry season and vice versa.

5. Discussion

[44] The dry season NIR reflectance (*BRF*) increase of 0.06 units, or about 23% (Figure 1), translates to a 16% increment in EVI (Figure 2), which is primarily sensitive to NIR (cf. Section 3.3), and this sensitivity increases with the magnitude of NIR reflectance (Figure 3). This change in EVI cannot be unambiguously interpreted because the exact property of the vegetation that this index measures is unknown. Another widely used index, the Normalized Difference Vegetation Index (NDVI), on the other hand, increases by only a small amount (4–5%) for the same increase in NIR reflectance (cf. Section 3.3), because its formulation is such that it dampens NIR reflectance changes and is independent of the magnitude of NIR reflectance (Figure 3). This NDVI change in absolute units is only 0.04, which is insignificant relative to the annual mean NDVI value of about 0.85 (Figure 2); this behavior is known as saturation in dense vegetation canopies, such as the Amazon forests. This rather small increase in NDVI, compared to a much larger increase in EVI, for the same change in canopy spectral reflectances further highlights the limitations of using vegetation indices for remote sensing of vegetation (as in work by *Huete et al.* [2006], *Xiao et al.* [2006], and *Brando et al.* [2010]).

[45] The MODIS LAI algorithm converts surface red and NIR reflectances and their overall uncertainties to most probable values of LAI [*Knyazikhin et al.*, 1998]. Uncertainties in surface reflectances include both observation and model uncertainties [*Wang et al.*, 2001]. The latter account for possible deviations of simulated reflectances from prescribed values in the look-up table due to variations in leaf optical properties. Thus, the algorithm converts surface spectral reflectances into LAI under the assumption that both leaf optical properties and LAI can vary (i.e., the impact function $k(\omega)$ is strictly positive, Section 3.4). Therefore, the algorithm is capable of detecting changes in leaf area. The MODIS algorithm reports approximately 18% increase in LAI (Figure 2) given the observed increase in NIR reflectance (Figure 1) during the dry season and a similar decrease in LAI during the wet season.

[46] New and mature leaves have leaf albedos (leaf reflectance plus transmittance) at NIR wavelengths that are 2–10% higher than those of older leaves due to aging and epiphyll cover [*Roberts et al.*, 1998; *Toomey et al.*, 2009]. The observed changes in NIR reflectance of Amazon forests (Figure 1) could be due to similar, but small, changes in NIR leaf albedos only, from exchanging older with newer leaves, with total leaf area unchanged, as argued by *Doughty and Goulden* [2008] and *Asner and Alencar* [2010] and confirmed by our analysis in Section 4.2.2. However, this ignores accumulating evidence from ground-based studies of higher leaf area in the dry season relative to the wet season, seasonal changes in litterfall and does not satisfactorily explain why NIR reflectance of these forests decreases in the following wet season. A more convincing explanation for the observed increase in NIR reflectance during the dry season and decrease during the wet season is one that invokes changes in both leaf area and leaf optical properties (Section 4.2.3). Such an argument is consistent with known phenological behavior of tropical forests (see the Introduction by *Myneni et al.* [2007]), ground-based reports of changes in leaf area [*Asner et al.*, 2004; *Carswell et al.*, 2002; *Pinto-Junior et al.*, 2010; *Malhado et al.*, 2009; *Negrón Juárez et al.*, 2009; *Doughty and Goulden*, 2008], litterfall [*Xiao et al.*, 2005; *Chave et al.*, 2010], leaf optical properties [*Roberts et al.*, 1998; *Toomey et al.*, 2009] and fluxes of evapotranspiration [*Juárez et al.*, 2007, 2008] and reconciles the various seemingly divergent views.

[47] A different line of reasoning on the cause of the dry season increase in NIR reflectance has been presented in a recent study by *Galvão et al.* [2011] using MODIS and hyperspectral (Hyperion and Hymap) data from a forest-savanna transitional site in Mato Grasso. The authors suggest that the dry season increase in NIR reflectance is caused by decreasing shade fraction resulting from large changes ($\sim$20°) in solar zenith angle (SZA), which in turn drives increase in EVI and MODIS LAI, given no observable changes in field-measured leaf area. While this study has correctly interpreted the increase in EVI arising from its dependence on NIR reflectance, the interpretation is based on correlation between the two rather than a thorough theoretical analysis presented here (cf. Section 3.3, Figure 3). The large SZA changes could be very specific to their study site because we have found significantly smaller changes in average SZA over Amazon forests (5°–6°, cf. Section 3.4.2). The suggestion that MODIS LAI changes are not representative of actual changes in leaf area is without basis because the MODIS LAI algorithm explicitly accounts for changes in SZA [*Knyazikhin et al.*, 1998] so as to preclude spurious LAI changes. Moreover, a large body of literature presents evidence of dry season leaf area increase [*Asner et al.*, 2004; *Carswell et al.*, 2002; *Pinto-Junior et al.*, 2010; *Malhado et al.*, 2009; *Negrón Juárez et al.*, 2009; *Doughty and Goulden*, 2008]. In addition, *Galvão et al.* [2011] did not examine the influence of leaf flush—leaf spectral changes—on NIR reflectance changes, which is presented here. All of these suggest that the results of *Galvão et al.* [2011] could be specific to their field site, as noted by the authors themselves, and may not be relevant to the vast expanse of Amazonian forests, the focus of our study.

[48] We have shown that the observed seasonal changes in NIR reflectance of Amazon forests are unlikely to be caused by changes in leaf area alone, but could, more plausibly, result from changes in both leaf area and leaf optical properties; however, our analysis is restricted to leaf optical property changes owing to leaf aging and epiphyll cover, given the paucity of literature on the sources of leaf optical property changes. The presence of a film of water on leaf surfaces, for instance due to a rainfall event, would tend to decrease greenness estimates because water reflects strongly

in red (blue) relative to NIR, an effect which is similar to the presence of residual atmospheric influences in the surface reflectances (cf. Figure S1). The use of VI error budget [from *Vermote and Kotchenova*, 2008] as an additional constraint on valid greenness increase in the dry season (cf. Figure 6 caption) would eliminate data showing such an effect. Among other possible causes of changes in leaf optical properties are leaf water content changes, dust coatings and coating with soot and carbonaceous particles emanating from biomass burning which is prevalent during the dry season. Thus, there is a need to explore these different mechanisms of leaf optical property variations. Finally, future research should also focus on spatial patterns of the causes (leaf area and leaf optical properties) of seasonal NIR reflectance variations of Amazonian forests.

[49] **Acknowledgment.** This work was supported by the NASA Earth Science Enterprise.

References

Aragao, L., Y. E. Shimabukuro, F. D. B. Espirito-Santo, and M. Williams (2005), Spatial validation of the collection 4 MODIS LAI product in Eastern Amazonia, *IEEE Trans. Geosci. Remote Sens.*, *43*(11), 2526–2534, doi:10.1109/TGRS.2005.856632.

Asner, G. P., and A. Alencar (2010), Drought impacts on the Amazon forest: The remote sensing perspective, *New Phytol.*, *187*(3), 569–578, doi:10.1111/j.1469-8137.2010.03310.x.

Asner, G. P., A. R. Townsend, and B. H. Braswell (2000), Satellite observation of El Niño effects on Amazon forest phenology and productivity, *Geophys. Res. Lett.*, *27*(7), 981–984, doi:10.1029/1999GL011113.

Asner, G. P., D. Nepstad, G. Cardinot, and D. Ray (2004), Drought stress and carbon uptake in an Amazon forest measured with spaceborne imaging spectroscopy, *Proc. Natl. Acad. Sci. U. S. A.*, *101*(16), 6039–6044, doi:10.1073/pnas.0400168101.

Brando, P. M., S. J. Goetz, A. Baccini, D. C. Nepstad, P. S. A. Beck, and M. C. Christman (2010), Seasonal and interannual variability of climate and vegetation indices across the Amazon, *Proc. Natl. Acad. Sci. U. S. A.*, *107*(33), 14,685–14,690, doi:10.1073/pnas.0908741107.

Carswell, F. E., et al. (2002), Seasonality in CO_2 and H_2O flux at an eastern Amazonian rain forest, *J. Geophys. Res.*, *107*(D20), 8076, doi:10.1029/2000JD000284.

Chave, J., et al. (2010), Regional and seasonal patterns of litterfall in tropical South America, *Biogeosciences*, *7*, 43–55, doi:10.5194/bg-7-43-2010.

Dessay, N., H. Laurent, L. A. T. Machado, Y. E. Shimabukuro, G. T. Batista, A. Diedhiou, and J. Ronchail (2004), Comparative study of the 1982–1983 and 1997–1998 El Niño events over different types of vegetation in South America, *Int. J. Remote Sens.*, *25*(20), 4063–4077, doi:10.1080/0143116031000101594.

Dickinson, R. E. (1983), Land surface processes and climate-surface albedos and energy balance, *Adv. Geophys.*, *25*, 305–353, doi:10.1016/S0065-2687(08)60176-4.

Doughty, C. E., and M. L. Goulden (2008), Seasonal patterns of tropical forest leaf area index and CO_2 exchange, *J. Geophys. Res.*, *113*, G00B06, doi:10.1029/2007JG000590.

Ferreira, L. G., and A. R. Huete (2004), Assessing the seasonal dynamics of the Brazilian Cerrado vegetation through the use of spectral vegetation indices, *Int. J. Remote Sens.*, *25*(10), 1837–1860, doi:10.1080/0143116031000101530.

Friedl, M. A., D. Sulla-Menashe, B. Tan, A. Schneider, N. Ramankutty, A. Sibley, and X. M. Huang (2010), MODIS Collection 5 global land cover: Algorithm refinements and characterization of new datasets, *Remote Sens. Environ.*, *114*(1), 168–182, doi:10.1016/j.rse.2009.08.016.

Fu, R., and W. Li (2004), The influence of land-surface on transition from dry to wet season in Amazonia, *Theor. Appl. Climatol.*, *78*, 97–110, doi:10.1007/s00704-004-0046-7.

Galvão, L. S., et al. (2011), On intra-annual EVI variability in the dry season of tropical forest: A case study with MODIS and hyperspectral data, *Remote Sens. Environ.*, *115*, 2350–2359, doi:10.1016/j.rse.2011.04.035.

Graham, E. A., S. S. Mulkey, K. Kitajima, N. G. Phillips, and S. J. Wright (2003), Cloud cover limits productivity in a tropical rain forest tree during La Nina, *Proc. Natl. Acad. Sci. U. S. A.*, *100*, 572–576, doi:10.1073/pnas.0133045100.

Huang, D., Y. Knyazikhin, W. Wang, D. W. Deering, P. Stenberg, N. Shabanov, B. Tan, and R. B. Myneni (2008), Stochastic transport theory for investigating the three-dimensional canopy structure from space measurements, *Remote Sens. Environ.*, *112*(1), 35–50, doi:10.1016/j.rse.2006.05.026.

Huete, A., K. Didan, T. Miura, E. P. Rodriguez, X. Gao, and L. G. Ferreira (2002), Overview of the radiometric and biophysical performance of the MODIS vegetation indices, *Remote Sens. Environ.*, *83*(1–2), 195–213, doi:10.1016/S0034-4257(02)00096-2.

Huete, A. R., K. Didan, Y. E. Shimabukuro, P. Ratana, S. R. Saleska, L. R. Hutyra, W. Z. Yang, R. R. Nemani, and R. Myneni (2006), Amazon rainforests green-up with sunlight in dry season, *Geophys. Res. Lett.*, *33*, L06405, doi:10.1029/2005GL025583.

Juárez, R. I. N., M. G. Hodnett, R. Fu, M. L. Goulden, and C. von Randow (2007), Control of dry season evapotranspiration over Amazonian forest as inferred from observations at a southern Amazon forest site, *J. Clim.*, *20*, 2827–2839, doi:10.1175/JCLI4184.1.

Juárez, R. I. N., et al. (2008), An empirical approach to retrieving monthly evapotranspiration over Amazonia, *Int. J. Remote Sens.*, *29*(24), 7045–7063, doi:10.1080/01431160802226026.

Knyazikhin, Y., J. V. Martonchik, R. B. Myneni, D. J. Diner, and S. W. Running (1998), Synergistic algorithm for estimating vegetation canopy leaf area index and fraction of absorbed photosynthetically active radiation from MODIS and MISR data, *J. Geophys. Res.*, *103*(D24), 32,257–32,275, doi:10.1029/98JD02462.

Knyazikhin, Y., L. Xu, M. A. Schull, R. B. Myneni, and A. Samanta (2010), Canopy spectral invariants. Part 1: A new concept in remote sensing of vegetation, *J. Quant. Spectrosc. Radiat. Transfer*, *112*, 727–735, doi:10.1016/j.jqsrt.2010.06.014.

Li, W., and R. Fu (2004), Transition of the large-scale atmospheric and land surface conditions from the dry to the wet season over Amazonia as diagnosed by the ECMWF Reanalysis, *J. Clim.*, *17*, 2637–2651, doi:10.1175/1520-0442(2004)017<2637:TOTLAA>2.0.CO;2.

Malhado, A. C. M., M. H. Costa, F. Z. de Lima, K. C. Portilho, and D. N. Figueiredo (2009), Seasonal leaf dynamics in an Amazonian tropical forest, *For. Ecol. Manage.*, *258*(7), 1161–1165, doi:10.1016/j.foreco.2009.06.002.

Myneni, R. B., F. G. Hall, P. J. Sellers, and A. L. Marshak (1995), The interpretation of spectral vegetation indexes, *IEEE Trans. Geosci. Remote Sens.*, *33*(2), 481–486, doi:10.1109/36.377948.

Myneni, R. B., et al. (2007), Large seasonal swings in leaf area of Amazon rainforests, *Proc. Natl. Acad. Sci. U. S. A.*, *104*(12), 4820–4823, doi:10.1073/pnas.0611338104.

NASA Land Processes Data Active Archive Center (LP DAAC) (2009), Land Cover Type Yearly L3 Global 1 km SIN Grid (MOD12Q1), https://lpdaac.usgs.gov/lpdaac/products/modis_products_table/land_cover/yearly_l3_global_1km2/mod12q1, USGS EROS Data Cent., Sioux Falls, S. D.

NASA Land Processes Data Active Archive Center (LP DAAC) (2010a), Vegetation Indices 16-Day L3 Global 1 km (MOD13A2), https://lpdaac.usgs.gov/lpdaac/content/view/full/6648, USGS EROS Data Cent., Sioux Falls, S. D.

NASA Land Processes Data Active Archive Center (LP DAAC) (2010b), Vegetation Indices 16-Day L3 Global 0.05deg CMG (MOD13C1), https://lpdaac.usgs.gov/content/view/full/6661, USGS EROS Data Cent., Sioux Falls, S. D.

NASA Land Processes Data Active Archive Center (LP DAAC) (2010c), Leaf Area Index–Fraction of Photosynthetically Active Radiation 8-Day L4 Global 1 km (MOD15A2), https://lpdaac.usgs.gov/lpdaac/products/modis_products_table/leaf_area_index_fraction_of_photosynthetically_active_radiation/8_day_l4_global_1km/mod15a2, USGS EROS Data Cent., Sioux Falls, S. D.

Negrón Juárez, R. I., H. R. da Rocha, A. Figueira, M. L. Goulden, and S. D. Miller (2009), An improved estimate of leaf area index based on the histogram analysis of hemispherical photographs, *Agric. For. Meteorol.*, *149*(6–7), 920–928, doi:10.1016/j.agrformet.2008.11.012.

Nemani, R. R., C. D. Keeling, H. Hashimoto, W. M. Jolly, S. C. Piper, C. J. Tucker, R. B. Myneni, and S. W. Running (2003), Climate-driven increases in global terrestrial net primary production from 1982 to 1999, *Science*, *300*(5625), 1560–1563, doi:10.1126/science.1082750.

Nepstad, D. C., C. R. Decarvalho, E. A. Davidson, P. H. Jipp, P. A. Lefebvre, G. H. Negreiros, E. D. Dasilva, T. A. Stone, S. E. Trumbore, and S. Vieira (1994), The role of deep roots in the hydrological and carbon cycles of Amazonian forests and pastures, *Nature*, *372*(6507), 666–669, doi:10.1038/372666a0.

Pinto-Junior, Q. B., L. Sanches, F. D. Lobo, A. A. Brandao, and J. S. Nogueira (2010), Leaf area index of a tropical semi-deciduous forest of the southern Amazon Basin, *Int. J. Biometeorol.*, *55*, 109–118, doi:10.1007/s00484-010-0317-1.

Rahman, A. F., D. A. Sims, V. D. Cordova, and B. Z. El-Masri (2005), Potential of MODIS EVI and surface temperature for directly estimating

per-pixel ecosystem C fluxes, *Geophys. Res. Lett.*, *32*, L19404, doi:10.1029/2005GL024127.

Rautiainen, M., M. Mottus, and P. Stenberg (2009), On the relationship of canopy LAI and photon recollision probability in boreal forests, *Remote Sens. Environ.*, *113*(2), 458–461, doi:10.1016/j.rse.2008.10.014.

Reich, P. B., C. Uhl, M. B. Walters, L. Prugh, and D. S. Ellsworth (2004), Leaf demography and phenology in Amazonian rain forest: A census of 40,000 leaves of 23 tree species, *Ecol. Monogr.*, *74*(1), 3–23, doi:10.1890/02-4047.

Roberts, D. A., B. W. Nelson, J. B. Adams, and F. Palmer (1998), Spectral changes with leaf aging in Amazon Caatinga, *Trees (Heidelberg, Ger.)*, *12*, 315–325, doi:10.1007/s004680050157.

Ross, J. (Ed.) (1981), *The Radiation Regime and Architecture of Plant Stands*, Dr. W. Junk, Boston, Mass.

Saleska, S. R., et al. (2003), Carbon in Amazon forests: Unexpected seasonal fluxes and disturbance-induced losses, *Science*, *302*(5650), 1554–1557, doi:10.1126/science.1091165.

Samanta, A., S. Ganguly, H. Hashimoto, S. Devadiga, E. Vermote, Y. Knyazikhin, R. R. Nemani, and R. B. Myneni (2010), Amazon forests did not green-up during the 2005 drought, *Geophys. Res. Lett.*, *37*, L05401, doi:10.1029/2009GL042154.

Samanta, A., S. Ganguly, and R. B. Myneni (2011a), MODIS Enhanced Vegetation Index data do not show greening of Amazon forests during the 2005 drought, *New Phytol.*, *189*(1), 11–15, doi:10.1111/j.1469-8137.2010.03516.x.

Samanta, A., M. H. Costa, E. L. Nunes, S. L. Vieira, L. Xu, and R. Myneni (2011b), Comment on "Drought-induced reduction in global terrestrial net primary production from 2000 through 2009", *Science*, *333*(6046), 1093, doi:10.1126/science.1199048.

Schull, M. A., et al. (2010), Canopy spectral invariants, Part 2: Application to classification of forest types from hyperspectral data, *J. Quant. Spectrosc. Radiat. Transfer*, *112*, 736–750, doi:10.1016/j.jqsrt.2010.06.004.

Schuur, E. A. G. (2003), Net primary productivity and global climate revisited: The sensitivity of tropical forest growth to precipitation, *Ecology*, *84*, 1165–1170, doi:10.1890/0012-9658(2003)084[1165:PAGCRT]2.0.CO;2.

Shabanov, N. V., et al. (2005), Analysis and optimization of the MODIS leaf area index algorithm retrievals over broadleaf forests, *IEEE Trans. Geosci. Remote Sens.*, *43*(8), 1855–1865, doi:10.1109/TGRS.2005.852477.

Sims, D. A., et al. (2008), A new model of gross primary productivity for North American ecosystems based solely on the enhanced vegetation index and land surface temperature from MODIS, *Remote Sens. Environ.*, *112*(4), 1633–1646, doi:10.1016/j.rse.2007.08.004.

Smolander, S., and P. Stenberg (2005), Simple parameterizations of the radiation budget of uniform broadleaved and coniferous canopies, *Remote Sens. Environ.*, *94*(3), 355–363, doi:10.1016/j.rse.2004.10.010.

Stenberg, P. (2007), Simple analytical formula for calculating average photon recollision probability in vegetation canopies, *Remote Sens. Environ.*, *109*(2), 221–224, doi:10.1016/j.rse.2006.12.014.

Toomey, M., D. Roberts, and B. Nelson (2009), The influence of epiphylls on remote sensing of humid forests, *Remote Sens. Environ.*, *113*(8), 1787–1798, doi:10.1016/j.rse.2009.04.002.

Vermote, E. F., and S. Kotchenova (2008), Atmospheric correction for the monitoring of land surfaces, *J. Geophys. Res.*, *113*, D23S90, doi:10.1029/2007JD009662.

Wang, Y. J., Y. H. Tian, Y. Zhang, N. El-Saleous, Y. Knyazikhin, E. Vermote, and R. B. Myneni (2001), Investigation of product accuracy as a function of input and model uncertainties: Case study with SeaWiFS and MODIS LAI/FPAR algorithm, *Remote Sens. Environ.*, *78*(3), 299–313, doi:10.1016/S0034-4257(01)00225-5.

Wright, S. J., and C. P. van Schaik (1994), Light and the phenology of tropical trees, *Am. Nat.*, *143*(1), 192–199, doi:10.1086/285600.

Würth, M. K. R., S. Peláez-Riedl, S. J. Wright, and C. Körner (2005), Non-structural carbohydrate pools in a tropical forest, *Oecologia*, *143*, 11–24, doi:10.1007/s00442-004-1773-2.

Xiao, X., et al. (2005), Satellite-based modeling of gross primary production in a seasonally moist tropical evergreen forest, *Remote Sens. Environ.*, *94*, 105–122, doi:10.1016/j.rse.2004.08.015.

Xiao, X. M., S. Hagen, Q. Y. Zhang, M. Keller, and B. Moore (2006), Detecting leaf phenology of seasonally moist tropical forests in South America with multi-temporal MODIS images, *Remote Sens. Environ.*, *103*(4), 465–473, doi:10.1016/j.rse.2006.04.013.

Xu, L., A. Samanta, M. H. Costa, S. Ganguly, R. R. Nemani, and R. B. Myneni (2011), Widespread decline in greenness of Amazonian vegetation due to the 2010 drought, *Geophys. Res. Lett.*, *38*, L07402, doi:10.1029/2011GL046824.

Yang, W., N. V. Shabanov, D. Huang, W. Wang, R. E. Dickinson, R. R. Nemani, Y. Knyazikhin, and R. B. Myneni (2006), Analysis of leaf area index products from combination of MODIS Terra and Aqua data, *Remote Sens. Environ.*, *104*(3), 297–312, doi:10.1016/j.rse.2006.04.016.

M. H. Costa, Federal University of Viçosa, Av. P. H. Rolfs, s/n, Viçosa, MG CEP 36570-000, Brazil.

R. E. Dickinson and R. Fu, Department of Geological Sciences, University of Texas at Austin, Austin, TX 78712, USA.

Y. Knyazikhin, R. B. Myneni, and L. Xu, Department of Geography and Environment, Boston University, Boston, MA 02215, USA.

R. R. Nemani, Biospheric Sciences Branch, NASA AMES Research Center, Moffett Field, CA 94035, USA.

S. S. Saatchi, Jet Propulsion Laboratory, California Institute of Technology, Pasadena, CA 91109, USA.

A. Samanta, Atmospheric and Environmental Research Inc., Lexington, MA 02421, USA. (arindam.sam@gmail.com)